LEADING EDGE VORTICES IN A CHORDWISE PERIODIC FLOW

M. Amitay, J. Er-El and A. Seginer
Faculty of Aerospace Engineering
Technion - Israel Institute of Technology
Haifa 32000, Israel.

Abstract

The flow over a slender delta wing in a periodically changing free-stream, is investigated theoretically and experimentally. The theoretical model assumes the wings to be slender and infinitesimally thin with straight spanwise cross-sections. The amplitudes and frequencies of the periodic motion are assumed to be very small so that the flow is governed by the steady two-dimensional Laplace equation. Time dependence is introduced through the boundary condition. The theoretical model was validated by the visualization of the flow over a delta wing in a periodic translational motion in a water tunnel. The vortical flow field over the wing was visualized by the hydrogen-bubbles technique. The spatial trajectories of the leading edge vortices as a function of several parameters, were found from the flow visualization results. Good agreement between the theoretical and the experimental results was found, as long as the small-perturbations assumption was justified. The results also show that the effects of a periodic flow are comparable with those of a periodically translating wing, under these assumptions and Galilei transformation.

Introduction

One of the concepts of increasing the performance envelope of future aircraft is super maneuverability. This concept which was introduced by Herbst [1], is based on recent developments in aircraft propulsion, control and aerodynamics. The contribution of aerodynamics to super maneuverability results from its unsteadiness. Numerous studies on unsteady-airfoil flows were carried out in the past, beginning with Theodorsen [2] and von Kármán and Sears [3]. Recent studies are motivated by super maneuverability. They are based on the observation that a pitching airfoil generates large-scale vortical structures (Helin and Walker, [4]). These structures can cause flow reattachment to the airfoil surface, even at post-stall angles. Walker and Chou [5] showed that these vortical structures induce an increased suction over the wing's upper surface, in a manner similar to the effects of the leading-edge vortices on a delta wing, and generate a large additional lift force. A theoretical model for a pitching slender wing at small amplitudes and frequencies was proposed by Randall [6]. Compared with the many studies of a pitching airfoil, relatively little work was done on unsteady chordwise motion. Lee et al. [7] tested a delta wing in a free stream with periodically changing velocity. Their measurements suggested that the unsteady lift coefficient reflected the free-stream acceleration.

This work presents a mathematical model for an infinitely thin, slender wing of a symmetric cross section in a periodically varying free-stream velocity with small amplitudes and frequencies. Such a wing is also tested experimentally in a chordwise periodic translational motion in a water tunnel. The mathematical model is an extension to unsteady flow of the Smith [8] model for slender wing in a steady flow. It is also based on the model of Randall [6] for slender wings that are pitching periodically with small amplitudes and frequencies. The present work deals with the influence of acceleration and deceleration of the free-stream on the position of the leading-edge vortices, the vortices strength and lift coefficient.

The Theoretical Model

Let x, $\hat{y}$, $\hat{z}$ be rectangular Cartesian coordinates, with their origin at the apex of the wing. The x-axis parallels the free-stream direction, the $\hat{z}$-axis lies in the plane containing the center line and the x-axis, and the $\hat{y}$-axis is chosen to complete a right-hand triad. The solution will be worked out in the cross-flow planes that are normal to the center line and contain the straight cross sections. The value of x that defines the cross-flow plane is a parameter only. Let y and z be Cartesian coordinates in the cross-flow plane with their origin at the intersection of this plane with the center line. The y-axis lies along the straight cross section, and the z-axis is perpendicular to the y-axis. y and $\hat{y}$ have the same direction and the direction of z and $\hat{z}$ differ by α. Figure 1 presents the coordinate systems.

Assuming now that the flow is irrotational, a velocity potential $\phi(x,\hat{y},\hat{z})$ exists such that the x, $\hat{y}$ and $\hat{z}$ components of the disturbance velocity (respectively u, $\hat{v}$ and $\hat{w}$) are given by

$$u = \frac{\partial\phi}{\partial x} \quad , \quad \hat{v} = \frac{\partial\phi}{\partial\hat{y}} \quad , \quad \hat{w} = \frac{\partial\phi}{\partial\hat{z}} \tag{1}$$

The linearized potential equation [9] of an unsteady flow (assuming that the disturbance velocities are very small compared with the free-stream velocity) is:

$$\frac{\partial^2\phi}{\partial x^2} + \frac{\partial^2\phi}{\partial\hat{y}^2} + \frac{\partial^2\phi}{\partial\hat{z}^2} = \frac{1}{a_0^2}\frac{\partial^2\phi}{\partial t^2} \tag{2}$$

For slender wings $\frac{\partial^2\phi}{\partial x^2} \ll \frac{\partial^2\phi}{\partial\hat{y}^2}, \frac{\partial^2\phi}{\partial\hat{z}^2}$ and for small amplitudes and frequencies $\frac{1}{a_0^2}\frac{\partial^2\phi}{\partial t^2} \ll \frac{\partial^2\phi}{\partial\hat{y}^2}, \frac{\partial^2\phi}{\partial\hat{z}^2}$, so that the governing equation becomes the steady two-

dimensional Laplace equation

$$\frac{\partial^2\phi}{\partial\hat{y}^2} + \frac{\partial^2\phi}{\partial\hat{z}^2} = 0 \tag{3}$$

Let Z denote the complex variable y+iz, where y_v+iz_v is the vortex position. It is expedient to introduce the transformation

$$Z^{*2} = Z^2 - c^2s^2 \tag{4}$$

In the Z*-plane the straight cross section becomes part of the imaginary axis so that $Z^*\to Z$ as $Z\to\infty$ (Fig. 2a).

The free-stream is time dependent and contains a steady and an unsteady component

$$U = U_0 + \varepsilon\cdot u(t) \tag{5}$$

where U_0 is the steady free-stream component, ε is a dimensionless quantity that is smaller than unity, and $\frac{u(t)}{U_0} \approx 1$.

The boundary conditions in the cross-flow plane: w=0 on the wing surface, and at infinity

$$w = \left[U_0 + \varepsilon\cdot u(t)\right]\alpha \tag{6}$$

determine the solution of Eq. (3). The complex potential in this case is given by [6]

$$W = -i\left[U_0 + \varepsilon\cdot u(t)\right]\alpha Z^* + \frac{\Gamma}{2\pi i}\ln\left(\frac{Z^*-Z_v^*}{Z^*+\bar{Z}_v^*}\right) \tag{7}$$

where Z* is defined by Eq. (4) and Γ is the vortex strength. Then "Kutta" condition, or the finite velocity at the leading-edges (Z=±cs), is determined in the transformation plane by dW/dZ*=0 at Z*=0. This means that Z*=0 is a stagnation point, and the boundary condition then is

$$\frac{\Gamma}{2\pi} = \frac{\alpha\left[U_0+\varepsilon\cdot u(t)\right]\bar{Z}_v^*Z_v^*}{Z_v^*+\bar{Z}_v^*} \tag{8}$$

In the steady case, the total force on the vortex and on the cut (here, the leading-edge vortex is replaced by a concentrated vortex and feeding sheet (Fig. 2b)) in the cross-flow planes must vanish, otherwise the vortex would not be stationary. The force acting on a length element d_ξ of the cut is

$$F_c = i\rho\frac{U}{c}d_\xi\left(Z_v-cs\right)\left[\Gamma' + \left(\frac{c}{U}\right)\dot{\Gamma}\right] \tag{9}$$

where dashes and dots denote differentiation with respect to ξ and t, respectively. This force is due to a pressure difference Δc_p across the cut. The force acting on a length element d_ξ of the vortex is

$$F_v = -i\rho\Gamma d_\xi\left\{v_1 - \frac{U}{c}\cdot\frac{\partial y_v}{\partial\xi} - \frac{\partial y_v}{\partial t} + i\left(w_1 - \frac{U}{c}\frac{\partial Z_v}{\partial\xi} - \frac{\partial Z_v}{\partial t}\right)\right\} \tag{10}$$

This force, known as the Magnus force, is the product of $-i\rho\Gamma d_\xi$ and the velocity perpendicular to the vortex at $Z=Z_v$. w_1 and v_1 are the velocity components at $Z=Z_v$ and are given by

$$v_1 - iw_1 = \left.\frac{dW_1}{d\bar{Z}}\right|_{Z=Z_v} \tag{11}$$

where W_1 is

$$W_1 = W - \frac{\Gamma}{2\pi i}\ln\left(Z-Z_v\right) \tag{12}$$

The condition that the total force vanishes results in

$$\frac{1}{\Gamma}\left\{\left(\bar{Z}_v-cs\right)\left[\left(U_0+\varepsilon\cdot u(t)\right)\Gamma' + c\dot{\Gamma}\right] + \Gamma\left[\left(U_0+\varepsilon\cdot u(t)\right)\bar{Z}_v' + c\dot{\bar{Z}}_v\right]\right\}$$

$$= \frac{c\Gamma}{2\pi i}\cdot\frac{Z_v}{\bar{Z}_v^*}\left\{\frac{Z_v^*+\bar{Z}_v^*}{Z_v^*\bar{Z}_v^*} - \frac{1}{Z_v^*+\bar{Z}_v^*} - \frac{c^2s^2}{2Z_v^2Z_v^*}\right\} \tag{13}$$

The term $\dot{\bar{Z}}_v$ is the temporal variation in the position of the vortex, and the term $\dot{\Gamma}$ expresses the variation in the pressure coefficient $\Delta c_p = -\left(\frac{2}{cU}\right)\left[\Gamma' + \left(\frac{c}{U}\right)\dot{\Gamma}\right]$. The unknown quantities Γ, Z_v and Z_v^* are replaced by the dimensionless quantities γ, m, q

$$\Gamma = 2\pi U_0 cs\gamma \tag{14a}$$

$$Z_v = csm \tag{14b}$$

$$Z_v^* = csq \tag{14c}$$

Substituting Eqs. (14) into Eqs. (4), (8) and (13) results in

$$q^2 = m^2 - 1 \tag{15a}$$

$$\gamma = \frac{\alpha\left[1+\varepsilon\cdot\frac{u(t)}{U_0}\right]q\cdot\bar{q}}{q+\bar{q}} \tag{15b}$$

$$s\left\{\left(\bar{m}-1\right)\left[\left(1+\varepsilon\cdot\frac{u(t)}{U_0}\right)\gamma' + \frac{c}{U_0}\dot{\gamma}\right] + \left(1+\varepsilon\frac{u(t)}{U_0}\right)\bar{m}' + \frac{c}{U_0}\dot{\bar{m}}\right\} + \gamma s'\left(1+\varepsilon\frac{u(t)}{U_0}\right)\left(2\bar{m}-1\right)$$

$$= \gamma^2 m\left\{\frac{2m^2q^3+2m^2q^2\bar{q}+2m^2\bar{q}^2q-q^2\bar{q}-q\bar{q}^2}{2im^2(q^4\bar{q}+q^3\bar{q}^2)}\right\} \tag{15c}$$

Let m, q and γ consist of a steady component and of a small unsteady one [6]

$$m = m_0(\xi) + \varepsilon\cdot m_1(\xi,t) \tag{16a}$$

$$q = q_0(\xi) + \varepsilon\cdot q_1(\xi,t) \tag{16b}$$

$$\gamma = \gamma_0(\xi) + \varepsilon\cdot\gamma_1(\xi,t) \tag{16c}$$

where the real and imaginary parts of the quantities in Eqs. (16a-b) are written as

$$m_0 = \eta_0 + i\zeta_0 \tag{17a}$$

$$m_1 = \eta_1 + i\zeta_1 \tag{17b}$$

$$q_0 = \sigma_0 + i\tau_0 \tag{17c}$$

$$q_1 = \sigma_1 + i\tau_1 \tag{17d}$$

Equations (16) are now substituted into Eqs. (15) and the resulting equations are expanded in powers of ε, where powers of ε higher than unity are neglected. It proves most convenient to choose q_1 for the dependent variable. From Eqs. (16a) and (16b) one obtains

$$m_0 m_1 = q_0 q_1 \tag{18a}$$

From Eqs. (16b), (16c) and (15b)

$$\gamma_1 = \frac{\gamma_0\bar{q}_0}{q_0(q_0+\bar{q}_0)}\,q_1 + \frac{\gamma_0 q_0}{\bar{q}_0(q_0+\bar{q}_0)}\,\bar{q}_1 + \gamma_0\frac{u(t)}{U_0} \tag{18b}$$

From Eqs. (15c), (16), (18a) and (18b)

$$\left(a_1+ib_1\right)q_1+\left(a_2+ib_2\right)\bar{q}_1+s\left(a_3+ib_3\right)\left(q_1'+\frac{c}{U_0}\dot{q}_1\right)+$$

$$+\,s\left(a_4+ib_4\right)\left(\bar{q}_1'+\frac{c}{U_0}\dot{\bar{q}}_1\right)=\left(a_5+ib_5\right)u(t)-s\left(a_6+ib_6\right)\dot{u}(t) \tag{18c}$$

where

$$a_1+ib_1 = 2im_0q_0^3\bar{q}_0\left(q_0+\bar{q}_0\right)\left[s\left(\bar{m}_0-1\right)\bar{A}'+s\left(2\bar{m}_0-1\right)\bar{A}\right]$$

$$+\;2i\left[s\gamma_0'\left(\bar{m}_0-1\right)+s\bar{m}_0'+s'\gamma_0\left(2\bar{m}_0-1\right)\right]\left(4m_0q_0^3\bar{q}_0+\frac{q_0^5\bar{q}_0}{m_0}+\right.$$

$$\left.+\;3m_0q_0^2\bar{q}_0^2+q_0^4\frac{\bar{q}_0^2}{m_0}\right)-\left[6m_0^2q_0^2\gamma_0^2+4q_0^4\gamma_0^2+4m_0^2\gamma_0^2q_0\bar{q}_0+\right.$$

$$+\;4q_0^3\gamma_0^2\bar{q}_0+2m_0^2\gamma_0^2\bar{q}_0^2+4\gamma_0^2q_0^2\bar{q}_0^2-\bar{q}_0^2\gamma_0^2-2\gamma_0^2q_0\bar{q}_0$$

$$\left.+\;2\gamma_0\bar{A}\left(2m_0^2q_0^3+2m_0^2q_0^2\bar{q}_0+2m_0^2\bar{q}_0^2q_0-\bar{q}_0^2q_0-q_0^2\bar{q}_0\right)\right] \tag{19a}$$

$$a_2+ib_2=2im_0q_0^3\bar{q}_0\left(q_0+\bar{q}_0\right)\left[s\left(\bar{m}_0-1\right)B'+s\gamma_0'\frac{\bar{q}_0}{\bar{m}_0}+\right.$$

$$+\;s\left(\frac{\bar{q}_0'}{\bar{m}_0}-\frac{\bar{m}_0'\bar{q}_0}{\bar{m}_0^2}\right)-\frac{2s'\gamma_0\bar{q}_0}{\bar{m}_0}+s\left(2\bar{m}_0-1\right)B\Big]+$$

$$+\;2i\left[s\gamma_0'\left(\bar{m}_0-1\right)+s\bar{m}_0'+s'\gamma_0\left(2\bar{m}_0-1\right)\right]$$

$$\cdot\left(m_0q_0^4+2q_0^3\bar{q}_0m_0\right)-\left[2m_0^2\gamma_0^2q_0^2+4m_0^2\gamma_0^2\bar{q}_0q_0-\gamma_0^2q_0^2-2\bar{q}_0q_0\gamma_0^2+\right.$$

$$\left.+\;2\gamma_0B\left(2m_0^2q_0^3+2m_0^2q_0^2\bar{q}_0+2m_0^2\bar{q}_0^2q_0-q_0^2\bar{q}_0-\bar{q}_0^2q_0\right)\right] \tag{19b}$$

$$a_3+ib_3 = 2i\bar{A}m_0q_0^3\bar{q}_0\left(q_0+\bar{q}_0\right)s\left(\bar{m}_0-1\right) \tag{19c}$$

$$a_4+ib_4 = 2im_0\bar{q}_0\left(q_0+\bar{q}_0\right)s\left[\left(\bar{m}_0-1\right)B+\frac{\bar{q}_0}{\bar{m}_0}\right] \tag{19d}$$

$$a_5+ib_5 = -\frac{2i\cdot m_0q_0^3\bar{q}_0\left(q_0+\bar{q}_0\right)}{U_0}\left[s\gamma_0'\left(\bar{m}_0-1\right)+s\bar{m}_0'\right.$$

$$\left.+\;2s'\gamma_0\left(2\bar{m}_0-1\right)\right]+$$

$$+\;\frac{2\gamma_0^2}{U_0}\left(2m_0^2q_0^3+2m_0^2q_0^2\bar{q}_0+2m_0^2\bar{q}_0^2q_0-q_0^2\bar{q}_0-\bar{q}_0^2q_0\right) \tag{19e}$$

$$a_6+ib_6=2im_0q_0^3\bar{q}_0\frac{c\gamma_0}{U_0^2}\left(q_0+\bar{q}_0\right) \tag{19f}$$

where

$$A \triangleq \frac{\gamma_0\bar{q}_0}{q_0(q_0+\bar{q}_0)} \qquad \text{and} \qquad B \triangleq \frac{\gamma_0 q_0}{\bar{q}_0(q_0+\bar{q}_0)}$$

Equation (18c) is a partial differential linear complex equation for q_1. Equations (17d) and (18c) result in:

$$\left(a_1+a_2\right)\sigma_1+\left(b_2-b_1\right)\tau_1+s\left(a_3+a_4\right)\sigma_1'+s\left(b_4-b_3\right)\tau_1'+$$

$$+\;\frac{sc}{U_0}\left(a_3+a_4\right)\dot{\sigma}_1+\frac{sc}{U_0}\left(b_4-b_3\right)\dot{\tau}_1=a_5u(t)-sa_6\dot{u}(t) \tag{20a}$$

$$\left(b_1+b_2\right)\sigma_1+\left(a_1-a_2\right)\tau_1+s\left(b_3+b_4\right)\sigma_1'+s\left(a_3-a_4\right)\tau_1'+$$

$$+\;\frac{sc}{U_0}\left(b_3+b_4\right)\dot{\sigma}_1+\frac{sc}{U_0}\left(a_3-a_4\right)\dot{\tau}_1=b_5u(t)-sb_6\dot{u}(t) \tag{20b}$$

Let us assume, with no loss of generality, that u(t) can be expressed as

$$u(t) = u_0e^{i\omega t} \tag{21a}$$

where

$$u_0 = \omega c \tag{21b}$$

Because Eqs. (20) are linear, σ_1 and τ_1 can be written in the form

$$\sigma_1(\xi,t) = \sigma_2(\xi)e^{i\omega t} \tag{22a}$$

$$\tau_1(\xi,t) = \tau_2(\xi)e^{i\omega t} \tag{22b}$$

Equations (20) and (21) yield two ordinary differential equations for σ_2 and τ_2:

$$\left[a_1+a_2+is\nu\left(a_3+a_4\right)\right]\sigma_2+\left[b_2-b_1+is\nu\left(b_4-b_3\right)\right]\tau_2+$$

$$+ s\left(a_3+a_4\right)\sigma_2'+s\left(b_4-b_3\right)\tau_2'=\left(a_5-is\omega a_6\right)\cdot u_0 \tag{23a}$$

$$\left[b_1+b_2+is\nu\left(b_3+b_4\right)\right]\sigma_2+\left[a_2-a_1+is\nu\left(a_3-a_4\right)\right]\tau_2+$$

$$+ s\left(b_3+b_4\right)\sigma_2'+s\left(a_3-a_4\right)\tau_2'=\left(b_5-is\omega b_6\right)\cdot u_0 \tag{23b}$$

where ν is the reduced frequency defined by

$$\nu = \frac{c\omega}{U_0} \tag{24}$$

It can be shown that the values of $\sigma_2(0)$ and $\tau_2(0)$ are obtained by solving

$$\left(b_1+b_2\right)\sigma_2 + \left(a_1-a_2\right)\tau_2 = b_5u_0 \tag{25a}$$

$$\left(a_1+a_2\right)\sigma_2 + \left(b_2-b_1\right)\tau_2 = a_5u_0 \tag{25b}$$

when the values of all the coefficients are taken at ξ=0.

Solution Process

The unsteady solution depends on the steady one because a_j, b_j j=1÷6 are functions of σ_0, τ_0, ζ_0, η_0 that are steady-state parameters. Therefore, the steady flow is calculated first, using Smith's model [8] and the unsteady flow solution follows. Equations (18a) and (22) define η_2 and ζ_2

$$\eta_1 = \frac{(\eta_0\sigma_0+\zeta_0\tau_0)\sigma_2-(\eta_0\sigma_0-\zeta_0\sigma_0)\tau_2}{\eta_0^2+\zeta_0^2}e^{i\omega t} = \eta_2e^{i\omega t} \tag{26a}$$

$$\zeta_1 = \frac{(\eta_0\tau_0-\zeta_0\sigma_0)\sigma_2-(\eta_0\sigma_0+\zeta_0\tau_0)\tau_2}{\eta_0^2+\zeta_0^2}e^{i\omega t} = \zeta_2e^{i\omega t} \tag{26b}$$

Equations (18b) and (22) define γ_2

$$\gamma_1=\left\{\frac{\gamma_0}{\sigma_0(\sigma_0^2+\tau_0^2)}\left[\sigma_2\left(\sigma_0^2-\tau_0^2\right)+2\sigma_0\tau_0\tau_2\right]+\gamma_0\frac{u_0}{U_0}\right\}e^{i\omega t}=\gamma_2e^{i\omega t} \tag{27}$$

The physical quantities are obtained by combining Eqs. (14a-b), (16a) and (16c):

$$y_v = cs\eta_0 + \varepsilon cs\eta_2e^{i\omega t} \tag{28a}$$

$$z_v = cs\zeta_0 + \varepsilon cs\zeta_2e^{i\omega t} \tag{28b}$$

$$\Gamma = 2\pi U_0cs\gamma_0 + \varepsilon\cdot 2\pi U_0cs\gamma_2e^{i\omega t} \tag{28c}$$

where η_2, ζ_2 are complex. The phase differences between the velocity and the variations of the vortex position and strength are given by:

$$\eta_2 = \left(\eta_{2r}^2+\eta_{2i}^2\right)^{1/2}\cdot e^{i\varphi_1} \quad ; \quad \varphi_1 = tg^{-1}\left(\frac{\eta_{2i}}{\eta_{2r}}\right) \tag{29a}$$

$$\zeta_2 = \left(\zeta_{2r}^2+\zeta_{2i}^2\right)^{1/2}\cdot e^{i\varphi_2};\varphi_2 = tg^{-1}\left(\frac{\zeta_{2i}}{\zeta_{2r}}\right) \tag{29b}$$

$$\gamma_2 = \left(\gamma_{2r}^2+\gamma_{2i}^2\right)^{1/2}\cdot e^{i\varphi_3} \quad ; \quad \varphi_3 = tg^{-1}\left(\frac{\gamma_{2i}}{\gamma_{2r}}\right) \tag{29c}$$

where φ_1, φ_2 and φ_3 are the phase differences between the velocity and η_2, ζ_2 and γ_2, respectively.

The Lift Coefficient

Randall [6] claims that Robinson and Laurmann [9] used the momentum theorem to calculate the lift on the wing, $L(\xi)$, up to station ξ

$$L(\xi) = -\rho\cdot R.P.\left\{U\int_C WdZ+c\int_0^{\xi}\left(\frac{\partial}{\partial t}\int_C WdZ\right)d\xi\right\} \tag{30}$$

where C is the contour $Z=Re^{i\theta}$, with R a constant and θ defined by $tg\theta=z/y$.

Introducing the complex potential, W, into Eq. (30) results in:

$$L(\xi) = \rho\pi c^2s^2U_0^2\left(\alpha+4\gamma_0\sigma_0\right) +$$

$$+ \varepsilon\cdot 4\rho\pi c^2s^2U_0u_0\left(\gamma_0\sigma_2+\gamma_2\sigma_0\right)e^{i2\omega t} +$$

$$+ \varepsilon\rho\pi U_0^2R_1e^{i(\omega t+\varphi)} \tag{31}$$

where

$$R_1 = \sqrt{c^4s^4\left[2\alpha\frac{u_0}{U_0}+4\left(\gamma_0\sigma_2+\gamma_2\sigma_0\right)\right]^2+\left\{\nu c^2\int_0^{\xi}s^2\left[\alpha\frac{u_0}{U_0}+4\left(\gamma_0\sigma_2+\gamma_2\sigma_0\right)\right]d\xi\right\}^2} \tag{32}$$

and

$$\varphi = tg^{-1}\left\{\frac{c^2s^2\left[2\alpha\frac{u_0}{U_0}+4\left(\gamma_0\sigma_2+\gamma_2\sigma_0\right)\right]}{\nu c^2\int_0^{\xi}s^2\left[\alpha\frac{u_0}{U_0}+4\left(\gamma_0\sigma_2+\gamma_2\sigma_0\right)\right]d\xi}\right\} \tag{33}$$

The first term in Eq. (31) is the steady component of the lift. The steady lift coefficient, C_{L_0}, of a delta wing is therefore

$$C_{L_0} = \frac{1}{2} AR\left(\alpha+4\gamma_0\sigma_0\right) \tag{34}$$

The unsteady lift coefficient is given by:

$$C_{L_\theta} = \frac{2\pi K U_0^2}{\left[U_0+\varepsilon\cdot u(t)\right]^2}\left(\alpha+4\gamma_0\sigma_0\right)+$$

$$+\ \varepsilon\left\{\frac{8\pi K U_0}{\left[U_0+\varepsilon\cdot u(t)\right]^2}\, u_0\left(\gamma_0\sigma_2+\gamma_2\sigma_0\right)e^{i2\omega t}+\right.$$

$$\left.+\ \frac{2\pi U_0^2 R_1}{\left[U_0+\varepsilon\cdot u(t)\right]^2 Kc^2}\, e^{i(\omega t+\varphi)}\right\} \tag{35}$$

where K is obtained from the wing's leading-edge equation.

Experimental Apparatus and Procedure

The experiments were conducted in a 22 cm x 22 cm x 70 cm test section water tunnel. The free-stream velocity was 18 cm/sec. The model was 1 mm thick with a root chord of 14 cm with sharp leading-edges swept 75 degs. The flow over the wing was visualized by the hydrogen-bubbles technique. The bubbles were generated by electrolysis over three thin platinum strips (each 0.2 mm thick, 4 mm wide and 40 mm long) were planted in the left leading-edge (Fig. 3) that were connected to the negative pole of a D.C. power source, and the tunnel wall served as the anode. The wing performed a sinusoidal translational motion that was driven by a 60 watt D.C. motor. The amplitude of the motion was controlled by an excenter with a variable eccentricity. The wing rode on a sled that moved parallel to the flow direction connected by a wire to the excenter. The frequency of the motion was controlled by the motor voltage. The motion-amplitude range was 0÷1.5 cm and the frequency range was 0.5÷2 Hz. The wing motion mechanism is shown in Fig. 4. The experiment were conducted at angles of attack of 10 and 15 degs. The test parameters are listed in Table 1.

The principal source of light used to alluminate the flow in the working section consisted of a 1000 watts lamp and a cooling system. Normally, the wing was viewed with a plane of light parallel to the wing (for side view visualization) and perpendicular to the wing (for top view visualization). The hydrogen bubbles were caught in a rolling motion generated by the leading edge, vortex shed from the edge of the wing. The spanwise and the vertical position of the leading-edge vortex were found by using a Video Position Analyzer (model VPA-1000). The VPA used to analyze the photographs taken by a video camera (model DXC-M2P SONY).

Results and Discussion

Out of the results of the many experiments, those at 15 deg angle of attack with an oscillation amplitude of A=0.75 cm and frequency of ω=0.66 Hz are shown in more detail. The root-chord based Reynolds number was 2.5×10^4. The vertical position of the vortex is shown in Fig. 5 and its spanwise position is presented in Fig. 6. A full cycle of the motion is shown in both figures. At t/T=0,1 (which is the center of the forward motion, where the velocity is at its maximum and the acceleration vanishes) the vortex is closest to the surface and nearest to the leading-edge. At the center of the rearward motion (t/T=0.5) where the velocity is at its minimum and the acceleration vanishes, the vortex is the farthest inward from the leading-edge and farthest from the surface. At the foremost point of the motion (t/T=0.25), at maximum deceleration and zero velocity, the vortex is roughly at the mid-position between the previous two. It is seen that at this time the vortex breaks down near the trailing edge. At the rear most point of the wing travel (t/T=0.75) when the wing is under maximum acceleration and at zero velocity, the vortex is almost at the same position as at t/T=0.25, but no breakdown is observable over the wing. It is clearly seen that the main effect of the translational motion is on the vertical position of the vortex.

Figure 7 compares the experimental with the results computed by the mathematical model previously described. Test conditions are identical to those in Figs. 5 and 6 show the displacement of the vortex from its steady-state position in the trailing edge plane (x/c=1) during a full cycle of the periodic motion. The agreement between theoretical and experimental results is good. The hysteresis loop in Fig. 7 shows that the major effect of the period motion is on the height of the vortex above the wing, and that its maximum displacement from its steady-state position is at t/T=0, 0.5 and 1. A comparison of the theoretical and experimental variation in the chordwise direction of the vertical and of the spanwise vortex position, is presented in Figs. 8 and 9 respectively at an angle of attack of 10 deg, a frequency of 1 Hz and motion amplitudes of 0.35, 0.75 and 1.1 cm. It can be seen that the theoretical model predicts quite well the spanwise variation of the vortex position. The prediction of the vertical variation of the vortex position is less satisfactory. This can probably be explained by the fact that the vertical variation is not small, whereas the theoretical model assumes small perturbations. Figures 8 and 9 present a monotonic increase in the displacement of the vortex along the chordwise direction. This also shows that there is a correlation between the amplitudes of the vortex motion and of the wing motion. This correlation lead to the plotting of the displacements of the vortex, normalized by the amplitude of the wing motion (Figs. 10, 11). This normalization collapsed all the data on a single curve. This result indicates a linear relationship between the relative displacement of the vortex position and the wing-motion amplitude. Such a relationship is shown in Figs. 12 and 13. The agreement between theory and experiment in the relation spanwise displacement is excellent (Fig. 13). A lesser agreement is found in the vertical displacement as discussed above.

Vortex Strength

The variation of the vortex circulation in the trailing-edge plane (x/c=1) over one cycle of the wing motion is shown in Fig. 14. The test conditions are: angle of attack of 10 deg, frequency of 1 Hz and motion amplitudes of 0.35, 0.75 and 1.1 cm. Increasing the amplitude of the wing motion at a given frequency, also increases the changes in the vortex strength. The relation between the amplitudes of the variation in the circulation and of the wing motion, seems to be linear (Fig. 15). The influence of the frequency of the wing motion on the circulation of the vortex in the trailing-edge plane over a full motion cycle is presented in Fig. 16. The test conditions are α=10 deg, a=1.1 cm and ω=0.66 Hz and 1 Hz. There seems to be a correlation between the vortex strength and the wing-motion frequency. The chordwise distribution of the circulation itself at various motion amplitudes is presented in Fig. 17. As expected, the circulation increases when the distance from the wing apex increases.

Unsteady-Lift Coefficient

The variation of the dynamic lift coefficient over one cycle of the wing motion at an angle of attack of 10 deg is shown in Fig. 18 at a constant frequency of 1 Hz and with the motion amplitude as parameters. The same variation, but at a constant motion amplitude of 1.1 cm with the motion frequency as a parameter, is presented in Fig. 19. The effects of the motion parameters on the dynamic lift coefficient are similar to those on the circulation. It is quite clear that the acceleration and deceleration of the wing should effect the lift force. However, the phase difference observed here indicates that the acceleration is not the only mechanism that effects the lift. This is even more strongly evident in Fig. 20 that compares the time histories of the dynamic lift increment and of the acceleration of the wing. Not only is there a phase difference, but also the character of the lift variation in the second half of the cycle differs considerably from that of the acceleration. These effects must be due to the displacement of the vortices, in addition to the wing acceleration.

Conclusions

The good agreement between the vortex unsteady position as predicted by the theoretical model and between the experimental results, validates both the theoretical model, and the assumption that the Galilean transformation can be used as long as the amplitudes of the motion of the wing, as well as its frequencies (and consequently its acceleration) are small. The above means that the theoretical model of a freestream flow with a periodic variation in its velocity (a not very practical possibility) can predict the results of a periodic variation in the flight speed of a wing as long as the perturbations from steady-state are small. With the above in mind, it can be concluded that a periodic variation in flying speed will affect the leading-edge vortex position above the wing as well as its circulation and the generated lift. Another conclusion is that the lift is influenced both by the acceleration of the wing themselves, as well as by the displacement of the vortex. It is suggested that the responses of the vortices and of the lift to the periodic speed variation can furnish at least a qualitative indication of the influence that sudden acceleration of deceleration of the aircraft might have over the lift.

References

1. Herbst, W., "Supermaneuverability", Proceedings of the Workshop on Unsteady Separated Flow, Air-Force Academy, Colorado Springs, CO, Aug. 1983, pp. 1-9.

2. Theodorsen, T., "General Theory of Aerodynamic Instability and Mechanism of Flutter", NACA R-496, 1935.

3. von Kármán, T. and Sears, W.R., "Airfoil Theory in Non-Uniform Motion", *J. of the Aeronautical Sciences*, **5**, 1938, pp. 379-390.

4. Helin, H.E. and Walker, J.M., "Interrelated Effects of Pitch Rate and Pivot Point on Airfoil Dynamic Stall", *AIAA Paper* 85-0130, 1985.

5. Walker, J.M., Seiler, F.J. and Chou, D., "Unsteady Surface Pressure Measurements on a Pitching Airfoil", *AIAA Paper 85-0532*, 1985.

6. Randall, D.G., "Oscillating Slender Wings with Leading-Edge Separation", *The Aeronautical Quarterly*, **XVII**, Nov. 1966, pp. 311-333.

7. Lee, M., Shin, C. and Ho, C.M., "Response of a Delta Wing in Steady and Unsteady Flows", *Proceedings of the Forum on Unsteady Flow Separation*, 1987, ASME Appl. Mechanic, Bioeng. and Fluid Mechanics Conf., Cincinnati, Ohio.

8. Smith, J.H.B., "A Theory of the Separated Flow from the Curved Leading Edge of a Slender Wing", *British A.R.C. R&M*, No. 3116, Nov. 1957.

9. Robinson, A. and Laurmann, J.A., "Wing Theory", *Cambridge University Press*, 1966, pp. 481-527.

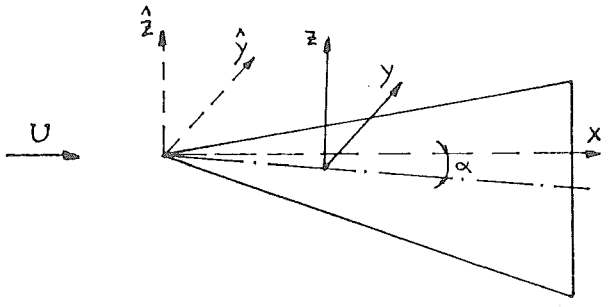

Fig. 1: Coordinate systems.

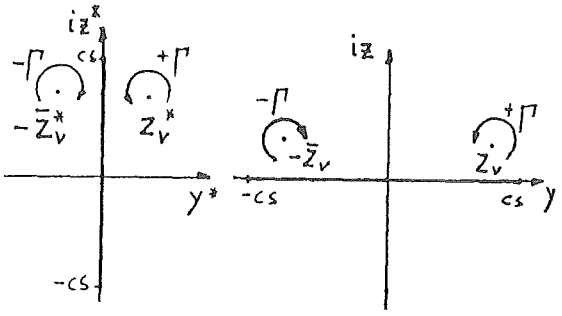

Fig. 2a: The physical plane and the transformation plane.

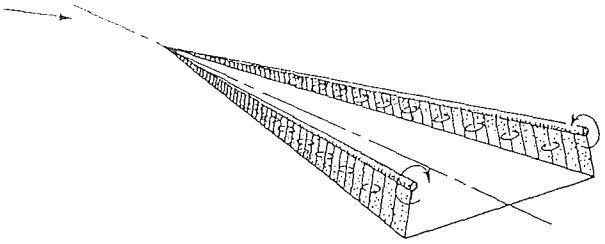

Fig. 2b: Approximated flow field.

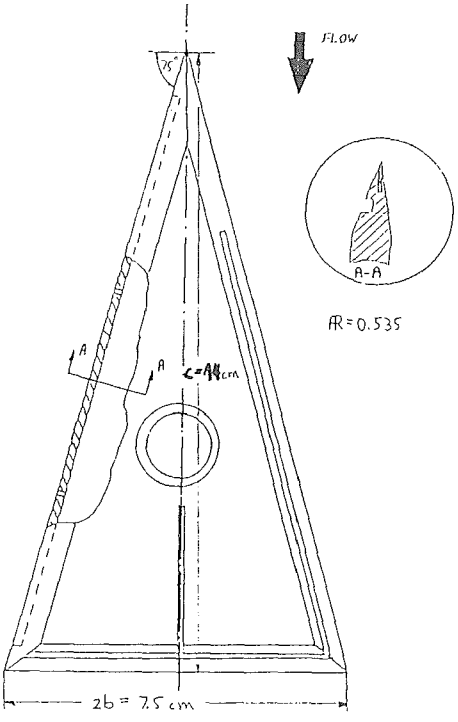

Fig. 3: The wing.

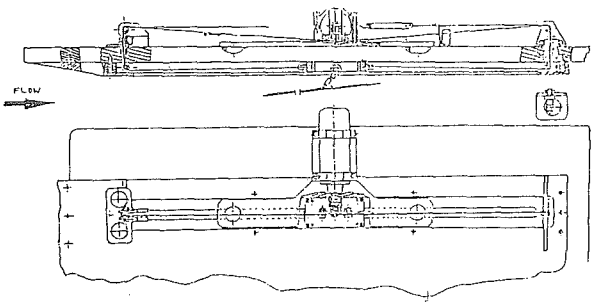

Fig. 4: The wing movement system.

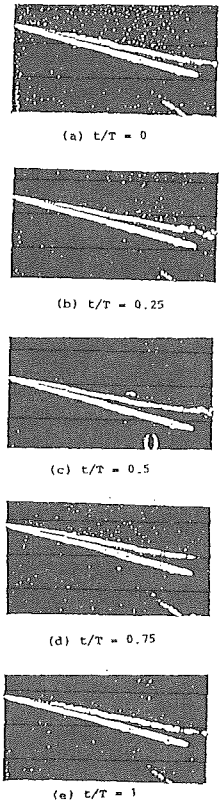

Fig. 5: Side view of the vortex over oscillating wing.

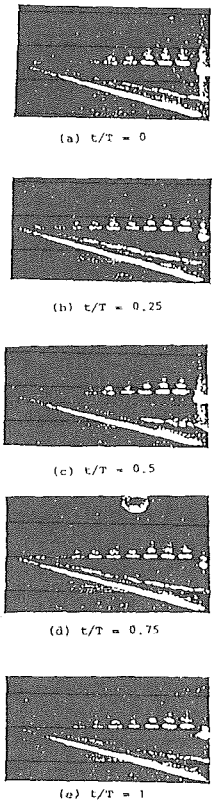

Fig. 6: Top view of the vortex over oscillating wing.

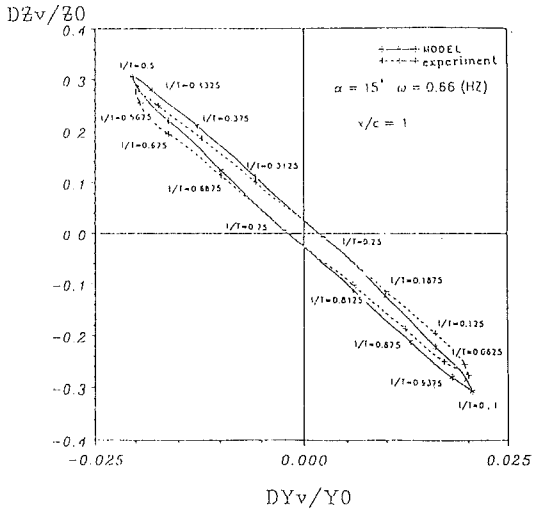

Fig. 7: Vortex-position variation at various times.

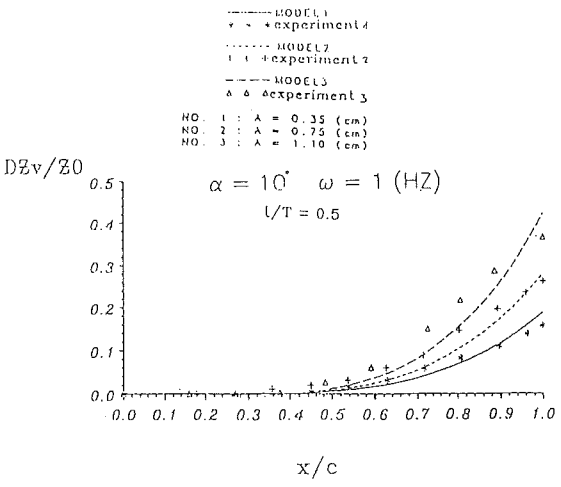

Fig. 8. Axial variation of the vertical L.E.-vortex position at various amplitudes.

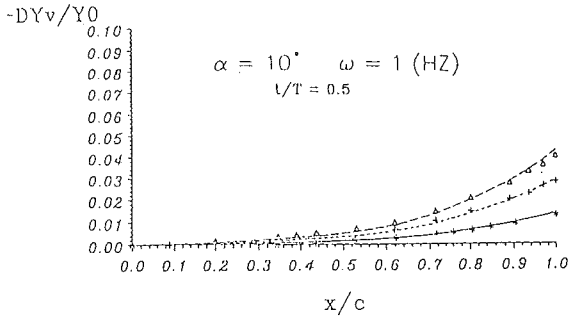

Fig. 9: Axial variation of the spanwise L.E.-vortex position at various amplitudes.

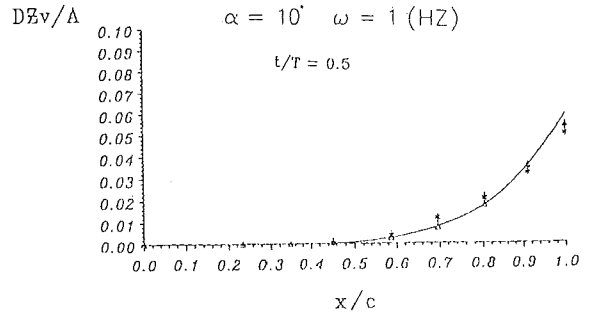

Fig. 10: Vertical vortex-position variation divided by the motion amplitude.

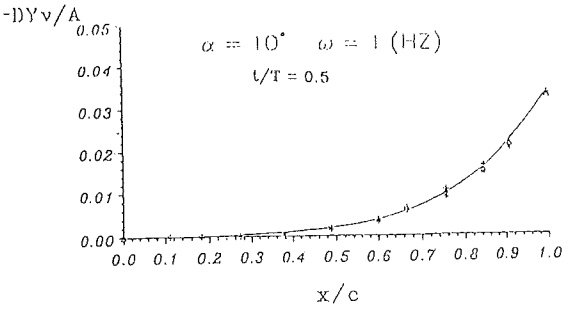

Fig. 11: Spanwise vortex-position variation divided by the motion amplitude.

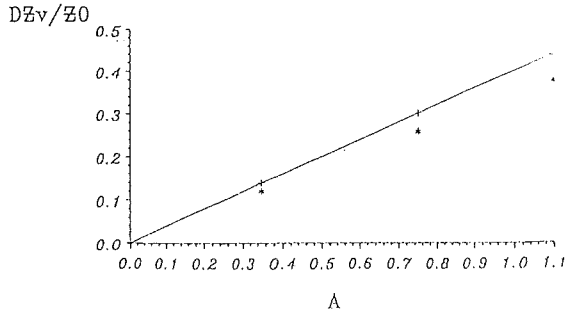

Fig. 12: Maximum vertical vortex position displacement at various amplitudes.

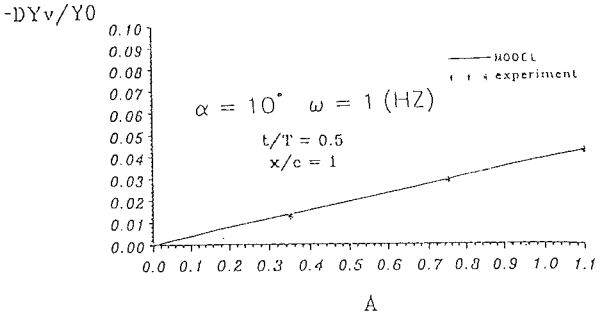

Fig. 13: Maximum spanwise vortex position displacement at various amplitudes.

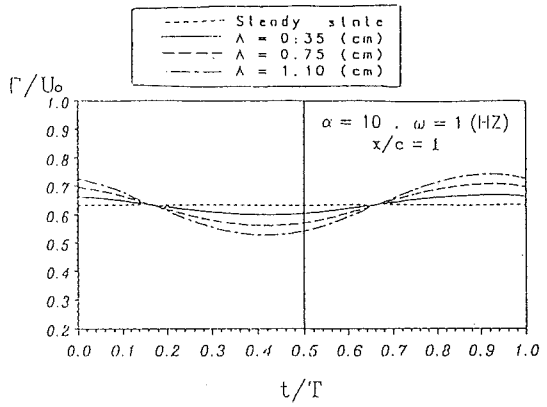

Fig. 14: Vortex strength at various amplitudes.

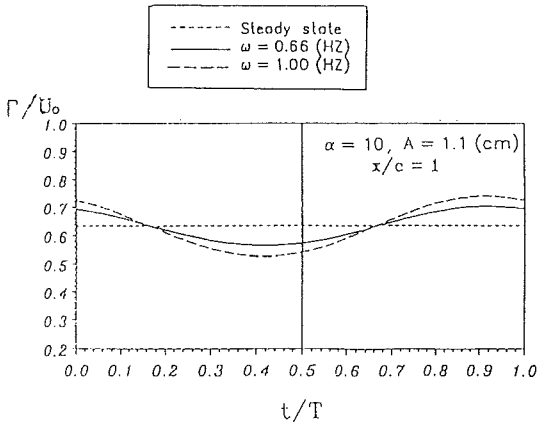

Fig. 15: Maximum vortex strength at various amplitudes.

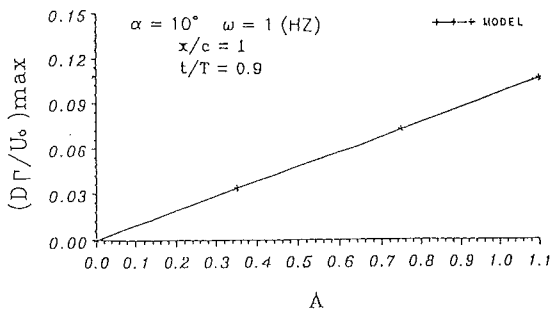

Fig. 16: Vortex strength at various frequencies.

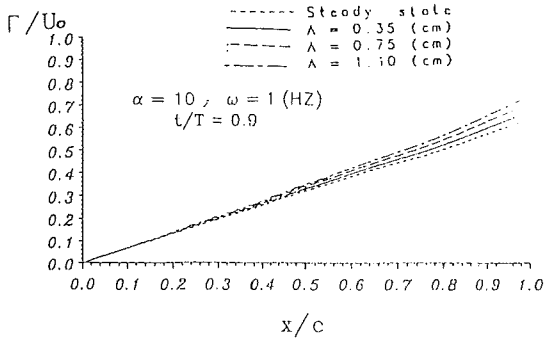

Fig. 17: Vortex strength distribution along the chord at various amplitudes.

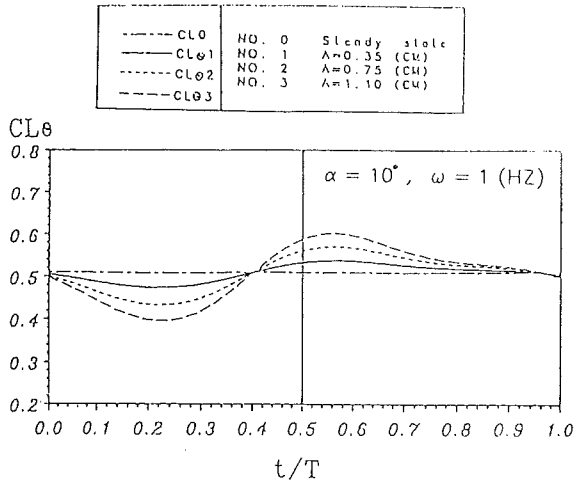

Fig. 18: Lift coefficient variation with time at various amplitudes.

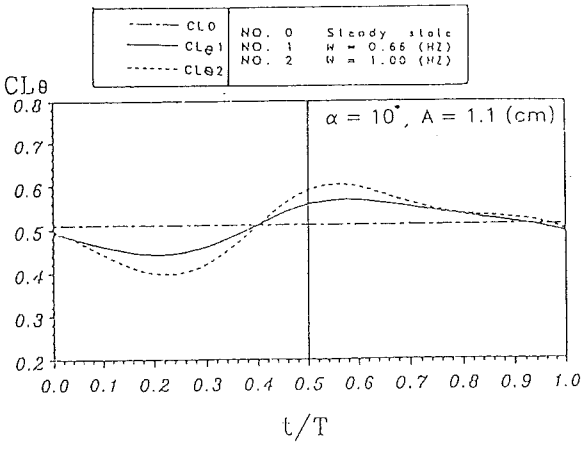

Fig. 19: Lift coefficient variation with time at various frequencies.

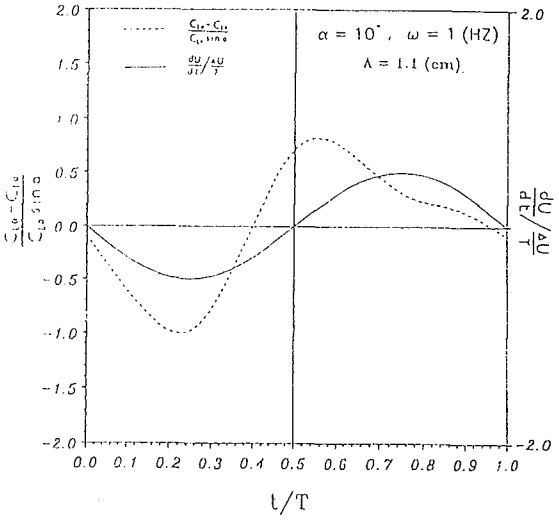

Fig. 20: Lift coefficient variation and acceleration vs. time.

Test No.	α°	ω(Hz)	A(cm)
1	10	0.66	0.35
2	10	0.66	0.75
3	10	0.66	1.10
4	10	1	0.35
5	10	1	0.75
6	10	1	1.10
7	15	0.66	0.35
8	15	0.66	0.75
9	15	0.66	1.10
10	15	1	0.35
11	15	1	0.75
12	15	1	1.10

Table 1: The list of the experiments.